

Fluid modeling of the laser ablation depth as a function of the pulse duration for conductorsS. Laville,¹ F. Vidal,¹ T. W. Johnston,¹ O. Barthélemy,² M. Chaker,¹ B. Le Drogoff,¹ J. Margot,² and M. Sabsabi³¹*Institut National de la Recherche Scientifique, Varennes, Québec, J3X 1S2 Canada*²*Université de Montréal, Montréal, Québec, H3C 3J7 Canada*³*Conseil National de Recherches du Canada, IMI, Boucherville, Québec, J4B 6Y4 Canada*

(Received 22 May 2002; published 26 December 2002)

Laser ablation of an aluminum target as a function of the pulse duration, for fluences up to 30 J/cm² and a wavelength of 0.8 μ m, is investigated by means of a fluid code. For a given fluence, the ablation depth shows a minimum for a pulse duration of ~ 10 ps between a maximum obtained for pulses shorter than ~ 1 ps and a lower maximum obtained for pulses in the nanosecond range, in qualitative agreement with published experimental results. The decrease in ablation depth with increase in pulse duration observed between 1 and 10 ps results from the reduced temperature rise near the surface due to increased inward heat transport. The increase in the ablation depth above ~ 10 ps is due to the increase in electron density gradient length while the laser pulse intensity is close to maximum, which thus enables the plasma to absorb more of the laser pulse energy for increased ablation.

DOI: 10.1103/PhysRevE.66.066415

PACS number(s): 52.38.-r, 79.20.Ds, 83.85.Pt

I. INTRODUCTION

Removal of matter by means of a laser beam, or laser ablation, is used in many applications including micromachining [1], thin film deposition [2], and chemical analysis [3]. The laser ablation dynamics depends strongly on the pulse duration. For subpicosecond laser pulses, most laser energy absorption occurs near the cold matter density since little matter displacement is possible during such a short pulse. The heated matter then expands nearly adiabatically. For longer pulse durations, significant heat conduction takes place inside the target while the matter is ablated and laser energy absorption occurs within the expanding plasma.

Several experimental papers have characterized the ablation depth (which is the one-dimensional equivalent of the amount of ablated matter) as a function of the pulse duration τ . The main conclusion of Ref. [4] is that the effective ablation depth per unit fluence in several metals as a function of the pulse duration shows two maxima. The highest maximum occurs for τ in the subpicosecond range and the smaller one occurs in the nanosecond range. The minimum occurs for τ in picoseconds. The same observations have been reported in Ref. [5], in the case of steel at high fluences ($\sim 10^2$ – 10^4 J/cm²). One can also deduce the same tendencies from the results of Ref. [6] for the ablation depth in copper as a function of the laser fluence (0–10 J/cm²) for various pulse durations. In Ref. [7], ablation experiments made with copper samples in the range 0–10 ps, at a fluence of 21 J/cm², clearly show a maximum in the ablation depth for subpicosecond pulses.

In Ref. [8] we had modeled the ablation process for a 500-fs laser pulse incident on aluminum using a fluid code which includes an equation-of-state (EOS) model (the model QEOS [9]) taking into account the unstable states of matter. (It has been assumed that the equilibrium vapor-liquid EOS, arranged according to the Maxwell construction, is not adequate for the fast phenomena of interest.) Our modeling showed that a clear separation between the ablated matter and the remaining target occurs as the ablated matter cools

down and reaches the critical point in the phase diagram. Near the critical point, the matter undergoes growing space density variations, which, in the framework of our one-dimensional model, can be interpreted as high-density droplets within a low-density plasma. This result seems to provide further justifications for the assumptions made in Ref. [10] to explain the annular interference patterns observed in their experiments.

The purpose of the present work is to investigate the dependence of the ablation depth as a function of the laser pulse duration by means of a fluid code similar to the one we used in Refs. [8,11]. It is shown here that our model can reproduce, at least qualitatively, the experimental behavior and help to provide a physical interpretation of the results. The discussion here is restricted to the case of an aluminum target, because this metal, which has a simple band structure, has been used to model successfully the absorption of subpicosecond laser pulses [8,12,13]. We also consider fluences not larger than 30 J/cm². For higher fluences, (such as those considered in Ref. [5]) effects not taken into account in our model, such as radiative losses and transfer, and radial plasma expansion, are probably very significant. Similar fluid modelings of the ablation depth have already been reported in Ref. [14]. While in that work the highest ablation depth occurred for subpicosecond pulses, in agreement with experiments, the chosen fluence (1.6 J/cm²) was presumably too small to show the most interesting experimental features.

The following section describes the model used in this paper, while Sec. III presents the simulation results. A discussion and the conclusion are given in Sec. IV.

II. THE MODEL

The code used here is a one-dimensional (1D) Lagrangian fluid code, which includes the EOS model QEOS [9]. The thermal and dc electrical conductivities are given by the model of Lee and More [15]. The laser field is modeled using the Helmholtz equation in which the complex ac electrical permittivity of the plasma is defined by means

of the Drude model. The model takes into account the counterpressure of a shock wave in an ambient gas by assuming that the shock is at equilibrium with the velocity of the plasma-gas interface. More details are given in Refs. [8,11].

In this paper, we take into account the fact that electrons and ions are not always at thermal equilibrium by solving the pair of temperature equations

$$\left(\frac{\partial U_x}{\partial T_x}\right)_\rho \frac{dT_x}{dt} + \left[\left(\frac{\partial U_x}{\partial \rho}\right)_{T_x} - \frac{p_x}{\rho^2}\right] \frac{d\rho}{dt} = S_x, \quad (1)$$

where the index x refers either to electrons (e) or the ion lattice (i). Here T_x is the temperature, U_x is the internal energy per unit mass, p_x is the pressure, and ρ is the mass density per unit volume (U_x and p_x are functions of T_e , T_i , and ρ given by the EOS model). The source terms are $S_i = Q_i + K_i$ and $S_e = H_e + X_e + K_e$. Here $H_e = \rho^{-1} \partial_z (\kappa_e \partial_z T_e)$ is the electron heat conduction term (ion thermal conduction is neglected), where z is the axial coordinate and the coefficient κ_e is given by the one-temperature ($T = T_e$) model of Lee and More [15]. In the above formulas, X_e is the laser-energy absorption rate, Q_i is the usual artificial viscosity term, and $K_e = -K_i$ is the energy exchange rate between electrons and the ion lattice. The latter term is expressed as $K_e = \rho^{-1} g (T_i - T_e)$, where $g = C_e / \tau_e$. Here $C_e = \rho (\partial U_e / \partial T_e)_\rho$ is the electron specific heat and τ_e is the mean energy exchange time for electrons in an ion-lattice background.

The determination of the coupling constant g in metals at solid density is a rather controversial subject and values differing by orders of magnitude can be found in the literature. For instance, in the case of aluminum, a value $g \approx 5 \times 10^{16} \text{ W m}^{-3} \text{ K}^{-1}$ has been estimated using strong shock wave radiation emission [16]. This value is about four times smaller than the value obtained in Ref. [13] by fitting short pulse absorption data, nearly ten times smaller than the value calculated in Ref. [17], and up to 20 times smaller than that used in Ref. [18] in their short pulse reflectivity simulations.

Instead of choosing a constant value for g at solid density in our simulations, we rather defined g by means of the above expression using a constant electron relaxation time in the solid, $\tau_{es} = 1$ ps. This value of τ_{es} is in agreement with measurements performed in gold up to $T_e = 1$ eV [19]. Similar relaxation times have also been found for different metals at lower temperatures [20,21]. The electron specific heat for aluminum at solid density, given by QEOS, can be approximated by $C_e \approx 3.2 \times 10^4 (T_e/300) \text{ J m}^{-3} \text{ K}^{-1}$ for temperatures T_e (in Kelvin) between room temperature and below a few eV. (For larger temperatures, C_e grows slower with respect to T_e .) This yields a coupling constant g that increases with the temperature [19], giving $\sim 3.2 \times 10^{16} \text{ W m}^{-3} \text{ K}^{-1}$ at room temperature and $\sim 10^{18} \text{ W m}^{-3} \text{ K}^{-1}$ at 1 eV. The latter value of g would likely be somewhat reduced if one tried to make corrections due to the band structure of aluminum, as done for gold in Ref. [19]. Although there is obviously much room for improvement in the determination of g near solid density, it is not the purpose of the present paper to solve this difficult issue. It should be mentioned that

most of our ablation depth calculations had also been done using $\tau_{es} \rightarrow 0$ (or $g \rightarrow \infty$), and only minor differences have been found with respect to the results presented here. However, the ablation thresholds presented in Sec. II B are somewhat more sensitive with respect to this parameter.

In the low-density plasma, we used an energy relaxation time $\tau_p m_i / 2m_e$, where τ_p is the mean collision time for momentum transfer in the low-density plasma, as given by the model of Lee and More, and m_i and m_e are the ion and electron masses, respectively. Since the energy relaxation time is in general too small when extrapolated to the cold solid, we have used the expression $\tau_e = \max(\tau_{es}, \tau_p m_i / 2m_e)$ for all temperatures and densities.

III. RESULTS

A. Plasma profiles

We show here a sample of the simulated plasma profiles which have been used to obtain the time-integrated quantities presented in this paper. In the example shown in Fig. 1, the Gaussian laser pulse has a fluence of 10 J/cm^2 and a full width at half maximum (FWHM) duration $\tau = 100$ ps. The plasma profiles are taken at the time $t = 250$ ps, the maximum intensity of the pulse being defined at $t = 200$ ps (i.e., at twice the FWHM after the sudden onset at $t = 0$). Figure 1(a) shows the electron density profile and the absorbed power as a function of the position z . The electron density profile decreases continuously from the solid density value $\sim 1.4 \times 10^{23} \text{ cm}^{-3}$ near $z = 0$ to a value of $n_s = 5.2 \times 10^{20} \text{ cm}^{-3}$ at $z = 2.82 \text{ } \mu\text{m}$. The absorbed power per unit volume, also represented in Fig. 1(a), shows a maximum near the plasma critical density, which is $n_c = 2.73 \times 10^{21} \text{ cm}^{-3}$ for the (Ti:Sapphire) laser wavelength $\lambda = 0.8 \text{ } \mu\text{m}$ of interest here. The absorbed power per unit volume shows oscillations with a period of approximately $\lambda/2$ (since the index of refraction is close to 1) due to interferences between the incident and the reflected laser fields. In most simulation results presented in this paper, more energy is absorbed within the bell-shaped absorption profile near the critical density than in the remaining underdense plasma.

Figure 1(b) shows the average degree of ionization, the electron and ion temperatures, and the plasma velocity as a function of position for the same time and the same laser parameters as in Fig. 1(a). The average degree of ionization $\langle Z \rangle$ is about 2.4 in the cold solid, as determined experimentally, and about 5 in the low-density plasma. The temperature profile has a maximum of about 12 eV in the low-density plasma and decreases continuously to the room temperature inside the target ($z < 0$), at some distance from the initial solid surface, due to thermal conduction. Differences between the electron and the ion temperature are rather small in the case shown here. The velocity is of the order of 10^4 m/s within the ablated matter, which corresponds approximately to the plasma sound velocity $c_s = \sqrt{5(1 + \langle Z \rangle) T_e / 3m_i}$. At $z \approx -0.6 \text{ } \mu\text{m}$, one observes the front of a weak shock wave, propagating to the left, inside the target.

For subpicosecond laser pulses, the plasma profiles are qualitatively similar to those shown in Fig. 1 [11] except that

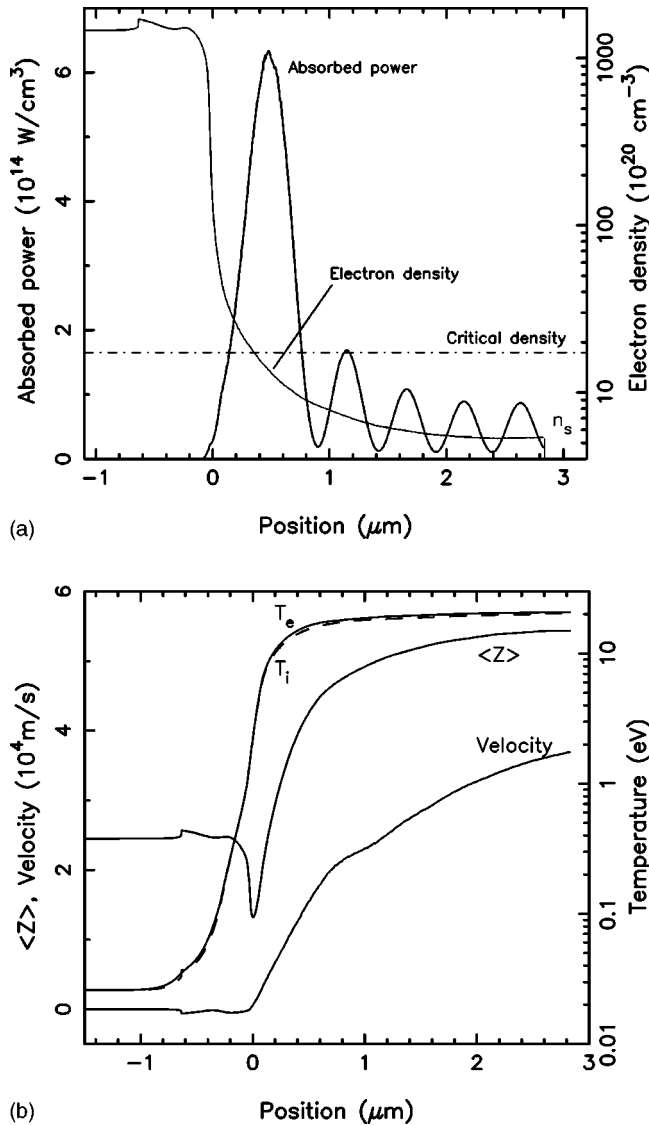


FIG. 1. (a) Electron density and absorbed power per unit volume as a function of position. n_s is the height of the electron density step in front of the plasma. (b) Electron temperature (T_e), ion temperature (T_i), plasma velocity, and average ionization ($\langle Z \rangle$) as a function of position z . The profiles are taken at the time $t = 250$ ps while the maximum intensity of the pulse is defined at $t = 200$ ps. The solid surface was initially at $z = 0$. The laser pulse is characterized by a duration of 100 ps and a fluence of 10 J/cm^2 .

most laser energy is absorbed before ablation begins and larger differences are observed between T_e and T_i during the laser pulse.

Taking into account an ambient gas (such as air) at a pressure ranging from zero to the atmospheric pressure has practically no influence on the results presented in this paper. This is due to the fact that the plasma pressure is much larger than the shock wave pressure for the early times considered here. However, later on, when the plasma pressure decreases, the air at atmospheric pressure restrains the plasma expansion to a few millimeters [11], in agreement with measurements. The discontinuities in front of the plasma profiles shown in Fig. 1 (at $z = 2.82 \mu\text{m}$) are a consequence of the

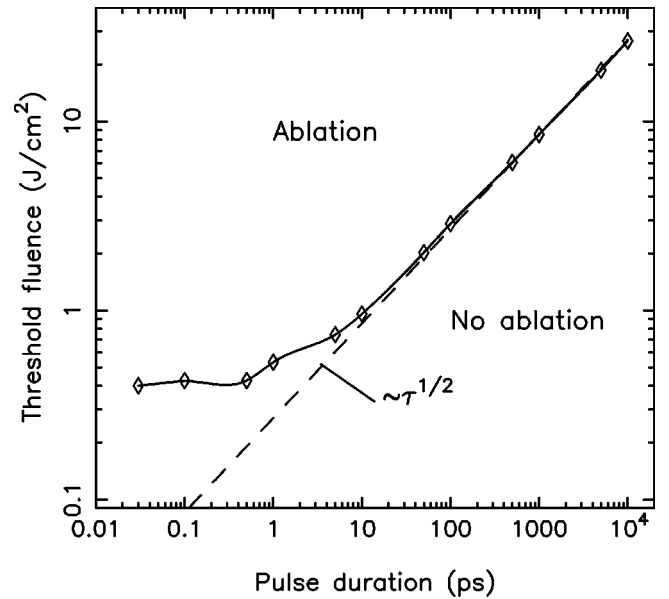


FIG. 2. Threshold fluence for ablation as a function of the pulse duration τ .

fact that no mixing and heat conduction are allowed between the plasma and the ambient gas in our model. This point will be discussed further in Sec. III C.

B. Ablation threshold

An essential feature of laser ablation is the existence of a threshold fluence (which depends on the material, wavelength, and pulse duration) below which no ablation is possible. Figure 2 shows simulation results for the threshold fluence for ablation of aluminum as a function of the pulse duration τ . Matter is determined to be ablated when a sharp jump appears in the plasma density profile, as explained in Ref. [8]. One observes in Fig. 2 two distinct regimes, with a transition occurring between 1 and 10 ps. For subpicosecond pulses, the threshold fluence takes the constant value of $\sim 0.4 \text{ J/cm}^2$, while for pulses longer than ~ 10 ps, the threshold fluence rises as $\tau^{1/2}$. Figure 2 is in qualitative agreement with experimental results obtained for gold [22], fused silica, and calcium fluoride [23]. The value of the threshold fluence obtained here for subpicosecond laser pulses is within the range of the measurements made for various metals [24] while somewhat higher than for aluminum ($\sim 0.08 \text{ J/cm}^2$) [25].

The physical interpretation of the two regimes observed here follows a rationale similar to that used for the damage threshold (interpreted as a melting point threshold), investigated in [26], that shows the same qualitative behavior as in Fig. 2.

It is well known that the $\tau^{1/2}$ behavior of the damage threshold for long pulse duration is due to the thermal conduction inside the target which drains the heat from the target surface [27]. For later use, let us express the incident *instantaneous fluence* as $f(t) = Ft/\tau$ for $0 \leq t \leq \tau$ and $f(t) = F$ for $t \geq \tau$, where F is the fluence of the laser pulse. Let us also express the fluence absorbed in the matter as $Af(t)$

$\approx \rho_s C_i T(t) \eta(t)$, where ρ_s is the solid mass density, A is the fraction of the laser energy absorbed (hereafter called *total absorption coefficient*), C_i is the ion specific heat, $T(t)$ is the temperature, assumed uniform within the thermal conduction length $\eta(t) \approx \sqrt{2k_e t}$, where k_e is the electron thermal conductance. One obtains $T(t) \approx T_{max} \sqrt{t/\tau}$ for $0 \leq t \leq \tau$ and $T(t) \approx T_{max} \sqrt{\tau/t}$ for $t > \tau$, where $T_{max} = T(\tau) = AF/\rho_s C_i \sqrt{2k_e \tau}$ is the maximum temperature reached. This simple estimate indicates that, for a given value of AF , the maximum temperature near the target surface goes as $\tau^{-1/2}$. In the framework of our ablation model [8], the matter needs to be heated above the temperature T_c of the critical point (which is ~ 1 eV in the equation-of-state model QEOS) to be ablated. The threshold fluence must thus be proportional to $\tau^{1/2}$ to raise the temperature to the appropriate value.

The near constancy of the ablation threshold observed for short pulses is basically due to the fact that $\eta(\tau)$ is on the same scale as, or smaller than, $\eta(\tau_{es})$, so that the plasma characteristics and evolution will be nearly the same for $t \gtrsim \tau_{es}$ (provided the absorbed laser energy is nearly constant, which is the case here, as shown in Sec. III C) [26]. Therefore, the ablation threshold is expected to be rather constant provided $\tau \leq \tau_{es} = 1$ ps, as observed in Fig. 2. In the limiting case where $\tau_{es} \rightarrow 0$, i.e., within the framework of a one-temperature model, the ablation threshold would still show a deviation from the $\tau^{1/2}$ behavior for pulses short enough that $\sqrt{2k_e \tau} \leq \alpha^{-1}$ [22].

In the case of aluminum, our code indicates that $\alpha^{-1} \approx 12$ nm and $k_e \approx 1.7 \times 10^{-4}$ m²/s at solid density for temperatures near $T_c \approx 1$ eV. One obtains $\sqrt{2k_e \tau_{es}}/\alpha^{-1} \approx 1.5$. The fact that this ratio is close to 1 explains why most results presented in this work are not much influenced by the use of either $\tau_{es} = 1$ ps or $\tau_{es} = 0$. When using $\tau_{es} = 0$, Fig. 2 remains qualitatively the same although the ablation threshold for short pulses is somewhat higher (~ 0.7 J/cm² at 100 fs) than the value obtained here, while still in reasonable agreement with experiments [24]. The explanation for this higher threshold seems to be that less laser energy is absorbed in the latter case at low fluences.

C. Ablation depth

Figure 3 shows the ablation depth of aluminum as a function of the pulse duration as obtained by our model for various fluences. One observes that the general shape of the curves for fluences higher than 10 J/cm² are in qualitative agreement with the experimental results described in Sec. I. For the fluences of 10, 20, and 30 J/cm², one can distinguish four main regions denoted with Roman numbers. A minimum in the ablation depth occurs between regions II ($1 \leq \tau \leq 10$ ps) and III ($10 \leq \tau \leq 10^3$ ps). The relative constancy of the ablation depth in region I ($\tau \leq 1$ ps) is explained by the same arguments as those used in Sec. III B for the threshold fluence in the range $\tau \leq \tau_{es}$. The decrease of the ablation depth in region IV ($\tau \gtrsim 10^3$ ps) is obviously due to the fact that for the given fluence, the pulse duration passes eventually in the region, shown in Fig. 2, where no ablation is possible.

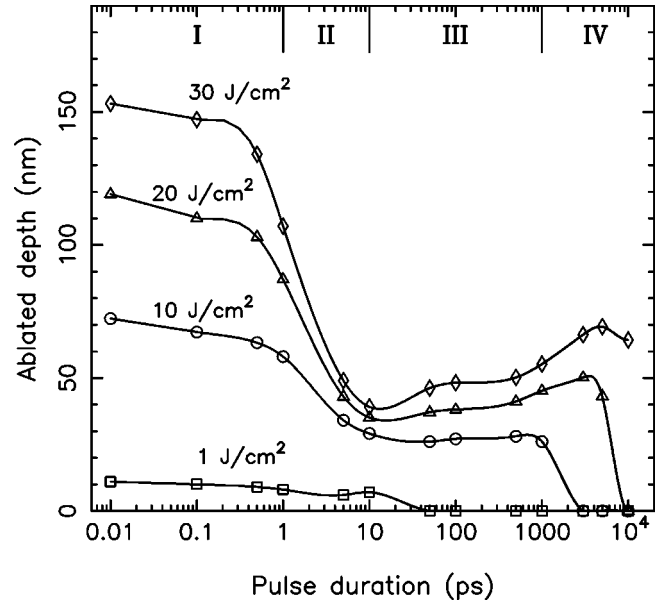


FIG. 3. Ablation depth as a function of the pulse duration for different fluences.

In order to understand regions II and III, let us express the ablation depth as $\delta_a = \tau_a v_a$ where τ_a is the duration of the ablation process and v_a is the velocity of the matter ablated from the surface, which can be estimated as $\sim \sqrt{T_{max}/m_i}$. The time τ_a is approximately the time during which the temperature at the target surface remains above the temperature T_c of the material critical point. Let us assume for simplicity that the pulse duration is not much larger than τ_{es} or that the fluence is close to threshold, so that one can still assume that most part of the absorbed laser energy lies in the solid target with the mass density ρ_s . Using the estimate of Sec. III B for the temperature, one obtains $\tau_a \approx \tau_f (1 - \tau^2/\tau_f^2)$, where $\tau_f = (AF/T_c \rho_s C \sqrt{k_e})^2$ is the time when ablation ends (i.e., when $T = T_c$ for $t > \tau$). One then finds that τ_a , v_a , and δ_a all increase as AF increases and decrease as τ increases.

In order to apply these considerations to the interpretation of Fig. 3, one must examine the total absorption coefficient A defined as

$$A = F^{-1} \int_0^{\infty} I(t) a(t) dt, \quad (2)$$

where $I(t)$ is the laser intensity and $a(t)$ is the *instantaneous absorption coefficient*. Note that $a(t)$, at a given instant t , depends only on the plasma profiles and on the laser wavelength. Figure 4 shows our simulation results for the total absorption coefficient A as a function of the pulse duration. One observes that A is rather constant in regions I and II, increases in region III, and decreases significantly in region IV. Beyond region IV the laser pulse is nearly completely reflected at the target surface, since the fluence is smaller than the threshold fluence and no plasma is created. From the above estimates and the near constancy of the total absorption coefficient in regions I and II, one concludes that the ablation depth should decrease in region II, as is effectively

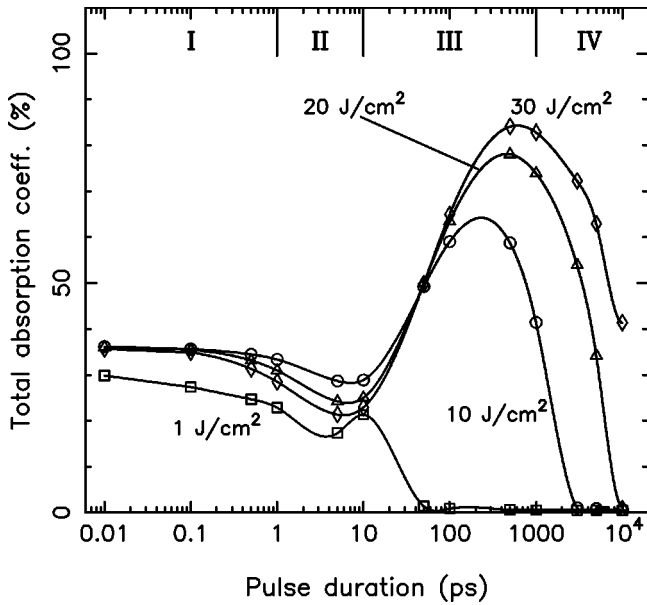


FIG. 4. Fraction of the laser energy absorbed as a function of the laser pulse duration for different fluences.

observed in Fig. 3. The increase of the ablation depth in region III can be explained by the increase of the absorption observed in Fig. 4.

The increase of the absorption in region III can be understood by examining the electron density profiles as a function of time obtained in our simulations. Simulations show that the electron density step of height n_s in front of the plasma [see Fig. 1(a)] starts from the electron density in the cold solid, at $t=0$, and becomes eventually smaller than n_c as the plasma expands. For the parameters of Fig. 1 this event occurs at the *critical time* $t_c=162$ ps. At that time, the electron density gradient length $\Lambda(t) \equiv |\partial_z \ln(n_e)|_{n_e=n_c}^{-1}$ at the plasma critical density (n_e is the electron density) changes abruptly from zero to a finite value. The analytical investigations of Ref. [28], connecting Λ and the instantaneous absorption a (made, however, for electron density profiles simpler than those of interest here), indicate that the plasma absorption increases with Λ/λ , which suggests that in our case the plasma absorbs the incoming laser energy more efficiently when $t \geq t_c$. This translates in an increase of $a(t)$.

Instead of trying to demonstrate this point by means of a tedious quasianalytical calculation, we illustrate it by means of an example drawn from the code. Figure 5 shows simulation results for the instantaneous absorption coefficient $a(t)$ as a function of time for the laser parameters of Fig. 1. One observes that, as stated above, $a(t)$ becomes significant for $t \geq t_c = 162$ ps. Actually, $a(t)$ starts increasing somewhat before t_c (i.e., at $t \approx 130$ ps) because the laser energy absorption takes place within a relatively large region around the critical density, compared with the size of the plasma, as shown in Fig. 1(a).

Figure 6 shows the critical time t_c extracted from the code as a function of 2τ , the time when the maximum intensity of the Gaussian laser pulse is achieved. This critical time t_c is the time at which our first plasma slice becomes underdense,

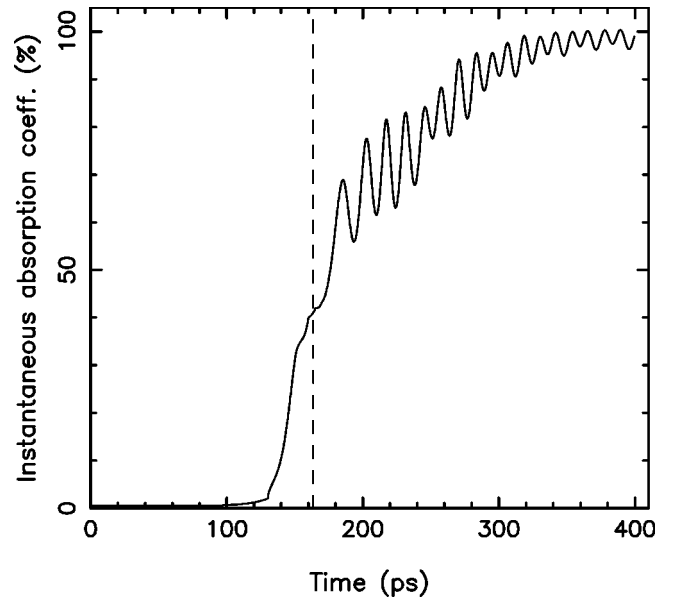


FIG. 5. Instantaneous absorption coefficient $a(t)$ as a function of time for a laser pulse with the parameters of Fig. 1. The vertical dashed line, at $t=162$ ps, denotes the critical time t_c , i.e., when $n_s = n_c$.

i.e., when its electron density falls below n_c . Figure 6 is for 10 J/cm^2 but the results are essentially the same for 20 J/cm^2 and 30 J/cm^2 . One observes that for $\tau \leq 1$ ps, t_c is practically constant and larger than 2τ , indicating that the critical time occurs well after the peak of the pulse. However, for $\tau \geq 3$ ps, one observes that $t_c \approx 2\tau$, which means that $a(t)$ becomes significant near the time when the laser intensity $I(t)$ is maximum. Using Eq. (2), one can see that A is likely to increase when $a(t)$ and $I(t)$ overlap significantly, which is

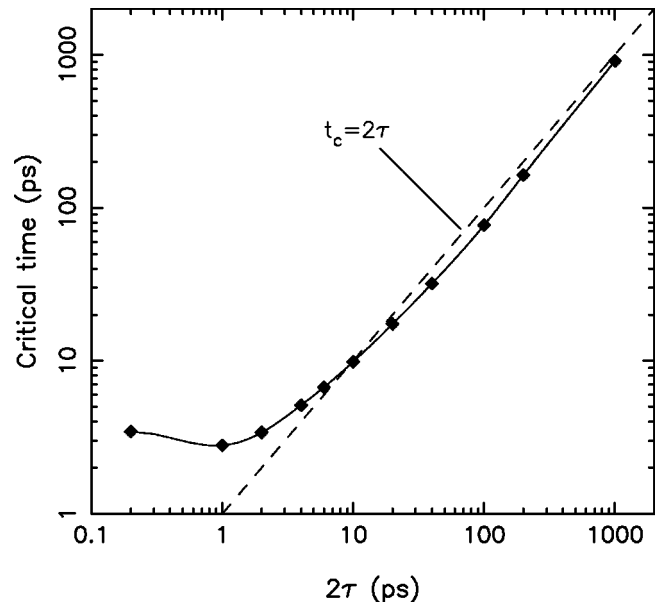


FIG. 6. Critical time t_c ($n_s = n_c$) as a function of two times the pulse duration τ (the time at which the maximum intensity of the laser pulse occurs) for a fluence of 10 J/cm^2 .

the case here when $\tau \gtrsim 3$ ps. This value is consistent with the onset of the increase of A (where $d^2A/d\tau^2 \approx 0$) in region II of Fig. 3.

To summarize the last argument, the increase of the ablation depth in region III is due to an increase in the total absorption A in that same region, as seen in Fig. 4. In turn, this increase in A is due to the increase in electron density gradient length $\Lambda(t)$ while the laser intensity is close to maximum (i.e., while much of the laser energy remains to be delivered), which thus enables the plasma to absorb more of the laser pulse energy.

In Fig. 6, the fact that $t_c > 2\tau$ for very short laser pulses was predictable because the matter does not have time to move during the laser pulse. The explanation for the constancy of t_c for $\tau \lesssim 1$ ps is the same as for the constancy of the threshold fluence (Fig. 3). The relation $t_c \approx 2\tau$ for $\tau \gtrsim 3$ ps observed in Fig. 6 is due to the fact that the ablation starts close to the maximum intensity of the pulse. Then the plasma expansion accelerates as the laser intensity increases and eventually the condition $n_s < n_c$ is met near the peak intensity of the pulse, at $t = 2\tau$.

The step in the electron density profiles at the front of the plasma is essential to our justification of the minimum in the ablated depth as a function of the pulse duration. Such a density discontinuity, though usual in fluid dynamics [29], is only an approximation in which the ion velocity departures from the mean value are neglected. The use of a kinetic model would reveal a transition over some finite width $\delta(t)$ in front of the plasma instead of the discontinuity obtained here. Unfortunately, convincing estimations of $\delta(t)$ would require detailed kinetic modeling, which would deserve a study by its own. This is particularly obvious in the case where the plasma expansion takes place in vacuum because $\delta(t)$ is determined by the particle velocity distribution near the front of the plasma. Even in the more straightforward case where the plasma expands in an ambient gas, an estimation of $\delta(t)$ is not without difficulty. Here the width $\delta(t)$ is determined by the plasma diffusion in the shocked and ionized part of the gas, i.e., $\delta(t) \approx \sqrt{Dt}$ where $D \approx v_{th}^2 \tau_c$ is the diffusion coefficient of the ablated ions in the ambient gas, v_{th} is the ion thermal velocity, and τ_c is the ion collision time in the shocked gas. (Note that for, say, $n_e = n_c$ and for a typical temperature of ~ 10 eV, the Debye length is smaller than 1 nm which is small compared with the size of the plasma, so that diffusion is ambipolar and thus controlled by the ions.) Estimating the plasma size as $L(t) \approx v_{th}t$, one gets $\delta/L \approx \sqrt{\tau_c/t}$. Unfortunately, an estimation of τ_c for the parameters of interest here (i.e., $n_e \approx n_c$, $\langle Z \rangle \approx 4$, $T \approx 10$ eV, ambient air at atmospheric pressure and singly ionized in the shocked part) yields a value for the Coulomb logarithm λ_C for the ion-ion interaction close to zero, which is far below

the allowable range of the usual formulas based on Maxwellian distributions and the weak coupling approximation [30]. Nevertheless, if one imposes a lower limit of 2 on λ_C , as done elsewhere for the electron-ion Coulomb logarithm [15], then one obtains $\tau_c \approx 2$ ps. Given this effective limit, one can thus indeed consider δ/L to be small when t is of the order of 10 ps, which corresponds to a value of $\tau = t/2$ in region II, where absorption starts increasing.

IV. CONCLUSION

This paper has presented simulation results and physical interpretations of the ablation depth as a function of the pulse duration. The ablation process appears to be the result of a competition between laser heating and thermal losses in the target. The latter increase as $\tau \gtrsim \tau_{es} = 1$ ps, i.e., as the pulse duration exceeds the electron-ion energy relaxation time. The increase in the ablation depth, starting at ~ 10 ps, is due to an increase in the plasma total absorption, in turn due to an increase in the electron gradient length near the plasma critical density while the laser intensity is close to maximum. Our simulations clearly indicate that the absorption of the laser energy by the expanding plasma *increases* the amount of ablated matter through thermal conduction toward the target surface, and does not prevent ablation as one might think.

While the code seems to include the essential physical mechanisms to reproduce qualitatively the experimental behavior, several factors indicate that the ablation depth could be somewhat underestimated in our simulations. For instance, there are evidences that in QEOS the critical temperature of aluminum is overestimated by a factor of about 2 [31]. As a consequence, more energy is required for ablation in the simulations, which results in an underestimation of the ablation depth. In addition, when much energy is absorbed in the expanding plasma, radiation emission (not taken into account here) from the hot low-density plasma could contribute, with the help of the normal thermal conduction, to heat up the high-density region where ablation takes place, thus increasing the ablation depth. However, the latter effect could be compensated by the transverse thermal losses in the target (not taken into account in our one-dimensional model) which could become important for long laser pulses, when the thermal conduction length becomes comparable to the focal spot diameter (i.e., $\sim \sqrt{2k_e\tau}$ in comparison to $\sim 10 \mu\text{m}$). Improvements to the model are currently in progress.

ACKNOWLEDGMENT

This work was financed partly by the National Science and Engineering Research Council of Canada (NSERC) under Strategic Grant No. STR 21898-98.

-
- [1] M. von Allmen and A. Blattner, *Laser-Beam Interaction with Materials, Physical Principles and Applications*, Springer Series in Materials Science, 2nd ed. (Springer, Berlin, 1995).
 [2] *Pulse Laser Deposition of Thin Films*, edited by D.B. Chrisey

and G. K. Hubler (Wiley, New York, 1994).

- [3] J.D. Winefordner, I.B. Gornushkin, D. Pappas, O.I. Matveev, and B.W. Smith, *J. Anal. At. Spectrom.* **15**, 1161 (2000).
 [4] A. Semerok, C. Chaléard, V. Detalle, J.-L. Lacour, P.

- Mauchien, P. Meynadier, C. Nouvellon, B. Sallé, P. Palianov, M. Perdrix, and G. Petite, *Appl. Surf. Sci.* **138-139**, 311 (1999).
- [5] C. Momma, B.N. Chichkov, S. Nolte, F. von Alvensleben, A. Tünnermann, H. Welling, and B. Wellegehausen, *Opt. Commun.* **129**, 134 (1996).
- [6] S. Nolte, C. Momma, H. Jacobs, A. Tünnermann, B.N. Chichkov, B. Wellegehausen, and H. Welling, *J. Opt. Soc. Am. B* **14**, 2716 (1997).
- [7] B. Sallé, O. Gobert, P. Meynadier, M. Perdrix, G. Petite, and A. Semerok, *Appl. Phys. A: Mater. Sci. Process.* **A69**, Suppl. S381 (1999).
- [8] F. Vidal, T.W. Johnston, S. Laville, O. Barthélemy, M. Chaker, B. Le Drogoff, J. Margot, and M. Sabsabi, *Phys. Rev. Lett.* **86**, 2573 (2001).
- [9] R.M. More, K.H. Warren, D.A. Young, and G.B. Zimmerman, *Phys. Fluids* **31**, 3059 (1988).
- [10] K. Sokolowski-Tinten, J. Bialkowski, A. Cavalleri, D. von der Linde, A. Oparin, J. Meyer-ter-Vehn, and S.I. Anisimov, *Phys. Rev. Lett.* **81**, 224 (1998).
- [11] F. Vidal, S. Laville, T.W. Johnston, O. Barthélemy, M. Chaker, B. Le Drogoff, J. Margot, and M. Sabsabi, *Spectrochim. Acta, Part B* **56**, 973 (2001).
- [12] A. Ng, P. Celliers, A. Forsman, R.M. More, Y.T. Lee, F. Perrot, M.W.C. Dharma-wardana, and G.A. Rinker, *Phys. Rev. Lett.* **72**, 3351 (1994).
- [13] K. Eidmann, J. Meyer-ter-Vehn, T. Schlegel, and S. Hüller, *Phys. Rev. E* **62**, 1202 (2000).
- [14] A.M. Komashko, M.D. Feit, A.M. Rubenchik, M.D. Perry, and P.S. Banks, *Appl. Phys. A: Mater. Sci. Process.* **A69**, Suppl. S95 (1999).
- [15] Y.T. Lee and R.M. More, *Phys. Fluids* **27**, 1273 (1984).
- [16] A. Ng, A. Forsman, and G. Chiu, *Phys. Rev. Lett.* **81**, 2914 (1998).
- [17] D. Fisher, M. Fraenkel, Z. Henis, E. Moshe, and S. Eliezer, *Phys. Rev. E* **65**, 016409 (2001).
- [18] X.Y. Wang and M.C. Downer, *Opt. Lett.* **17**, 1450 (1992).
- [19] X.Y. Wang, D.M. Riffe, Y.-S. Lee, and M.C. Downer, *Phys. Rev. B* **50**, 8016 (1994).
- [20] W.S. Fann, R. Storz, H.W.K. Tom, and J. Bokor, *Phys. Rev. B* **46**, 13 592 (1992).
- [21] H.E. Elsayed-Ali, T.B. Norris, M.A. Pessot, and G.A. Mourou, *Phys. Rev. Lett.* **58**, 1212 (1987).
- [22] P.P. Pronko, S.K. Dutta, D. Du, and R.K. Singh, *J. Appl. Phys.* **78**, 6233 (1995).
- [23] B.C. Stuart, M.D. Feit, A.M. Rubenchik, B.W. Shore, and M.D. Perry, *Phys. Rev. Lett.* **74**, 2248 (1995).
- [24] S. Preuss, A. Demchuk, and M. Stuke, *Appl. Phys. A: Mater. Sci. Process.* **A61**, 33 (1995).
- [25] B. Le Drogoff, F. Vidal, Y. von Kaenel, M. Chaker, T.W. Johnston, S. Laville, M. Sabsabi, and J. Margot, *J. Appl. Phys.* **89**, 8247 (2001).
- [26] P.B. Corkum, F. Brunel, N.K. Sherman, and T. Srinivasan-Rao, *Phys. Rev. Lett.* **61**, 2886 (1988).
- [27] H.S. Carslaw and J.C. Jaeger, *Conduction of Heat in Solids* (Clarendon, Oxford, 1959).
- [28] J.-C. Kieffer, J.-P. Matte, S. Bélair, M. Chaker, P. Audebert, H. Pépin, P. Maine, D. Strickland, P. Bado, and G. Mourou, *IEEE J. Quantum Electron.* **25**, 2640 (1989).
- [29] Y.B. Zel'dovich and Y.P. Raizer, *Physics of Shock Waves and High-Temperature Hydrodynamic Phenomena* (Academic, New York, 1967).
- [30] *NRL Plasma Formulary*, edited by J. D. Huba (Office of Naval Research, Washington, D.C., 2000).
- [31] A.V. Bushman, I.V. Lomonosov, and V.E. Fortov, *Equations of State of Metals at High Energy Densities* (Institute of Chemical Physics, Russian Academy of Sciences, Chernogolovka, 1992) (in Russian).